

# Structural Basis of Multisite Single-Stranded DNA Recognition and ACTA2 Repression by Purine-Rich Element Binding Protein B (Pur $\beta$ )

Amy E. Rumora,<sup>‡</sup> Shu-Xia Wang,<sup>§</sup> Lauren A. Ferris,<sup>‡</sup> Stephen J. Everse,<sup>‡</sup> and Robert J. Kelm, Jr.\*<sup>‡,§,||</sup>

<sup>‡</sup>Department of Biochemistry, <sup>§</sup>Department of Medicine, and <sup>||</sup>Cardiovascular Research Institute, University of Vermont College of Medicine, Burlington, Vermont 05405, United States

## S Supporting Information

**ABSTRACT:** A hallmark of dysfunctional fibroblast to myofibroblast differentiation associated with fibrotic disorders is persistent expression of *ACTA2*, the gene encoding the cyto-contractile protein smooth muscle  $\alpha$ -actin. In this study, a *PURB*-specific gene knockdown approach was used in conjunction with biochemical analyses of protein subdomain structure and function to reveal the mechanism by which purine-rich element binding protein B (Pur $\beta$ ) restricts *ACTA2* expression in mouse embryo fibroblasts (MEFs). Consistent with the hypothesized role of Pur $\beta$  as a suppressor of myofibroblast differentiation, stable short hairpin RNA-mediated knockdown of Pur $\beta$  in cultured MEFs promoted changes in cell morphology, actin isoform expression, and cell migration indicative of conversion to a myofibroblast-like phenotype. Promoter-reporter assays in transfected Pur $\beta$  knockdown MEFs confirmed that these changes were attributable, in part, to derepression of *ACTA2* transcription. To map the domains in Pur $\beta$  responsible for *ACTA2* repression, several recombinant truncation mutants were generated and analyzed based on hypothetical, computationally derived models of the tertiary and quaternary structure of Pur $\beta$ . Discrete subdomains mediating sequence- and strand-specific *cis*-element binding, protein–protein interaction, and inhibition of a composite *ACTA2* enhancer were identified using a combination of biochemical, biophysical, and cell-based assays. Our results indicate that the Pur $\beta$  homodimer possesses three separate but unequal single-stranded DNA-binding modules formed by subdomain-specific inter- and intramolecular interactions. This structural arrangement suggests that the cooperative assembly of the dimeric Pur $\beta$  repressor on the sense strand of the *ACTA2* enhancer is dictated by the association of each subdomain with distinct purine-rich binding sites within the enhancer.



The myofibroblast is a unique cell type that exhibits an ensemble of phenotypic properties typical of a collagenous matrix-producing fibroblast and a contractile smooth muscle cell.<sup>1</sup> In the body, preformed myofibroblasts play an important structural role in certain developing and adult tissues and organs.<sup>1,2</sup> On the other hand, emergent myofibroblasts are critical to the formation and remodeling of granulation tissue during wound healing because they provide the contractile machinery and mechanical strength necessary for wound closure.<sup>3–5</sup> While transient differentiation of resident connective tissue fibroblasts to myofibroblasts is a normal physiological response to tissue injury, persistent myofibroblast activation is associated with hypertrophic scarring, pathologic organ fibrosis, aberrant vascular remodeling, and dysfunctional stromal responses to neoplasia.<sup>6–9</sup> Consequently, an improved understanding of the molecular mechanisms underlying myofibroblast *trans*-differentiation may reveal novel drug targets to limit scarring, fibrosis, and tumor progression.

Among the markers of myofibroblast conversion, expression of *ACTA2*, the gene encoding smooth muscle  $\alpha$ -actin (SM $\alpha$ A)<sup>3</sup> is recognized as one of the key determinants of the transition to a contractile phenotype.<sup>10–12</sup> Based largely on comparing *ACTA2* reporter gene activity in myogenic versus nonmyogenic cell lines, early reports suggested that activation of *ACTA2* transcription in fibroblasts is mediated by serum-derived, growth factor-dependent signaling leading to induction of an

otherwise repressed 5' enhancer–promoter.<sup>13–15</sup> Later studies revealed that the 5' flanking region of *ACTA2* contains a variety of discrete but functionally interacting *cis*-elements that serve as binding sites for certain muscle-associated, growth factor-inducible, or basal *trans*-activators found in *ACTA2*-expressing fibroblasts.<sup>16–19</sup> In particular, combinatorial interactions between a transcription enhancer factor 1 (TEF1)-binding muscle CAT (MCAT) motif, two serum response factor (SRF)-interacting CArG boxes, and several specificity protein 1 and 3 (Sp1/3)-binding GC-rich elements are necessary to drive high level *ACTA2* transcription in differentiating myofibroblasts.<sup>17,20</sup> Conversely, in undifferentiated fibroblasts, the activity of a composite MCAT/CArG/GC box enhancer is apparently suppressed by several single-stranded DNA (ssDNA)-binding repressors that interact with the opposing strands of an asymmetric polypurine/polypyrimidine-rich (Pur/Pyr) tract containing the core MCAT motif.<sup>15,21</sup> Cell-based promoter mutagenesis studies in conjunction with nucleoprotein interaction analyses with double-stranded and single-stranded probes led to the identification of purine-rich element binding proteins A and B (Pur $\alpha$  and Pur $\beta$ ) and Y-box binding

Received: March 5, 2013

Revised: May 29, 2013

Published: June 3, 2013

protein 1 (YB-1) as the key factors in strand-specific Pur/Pyr tract recognition and repression of the composite ACTA2 enhancer.<sup>17,22</sup>

Pur $\alpha$  and Pur $\beta$  are members of a small family of nucleic acid-binding proteins that interact with purine-rich ssDNA or RNA sequences homologous to the so-called PUR element originally described in eukaryotic gene flanking regions and origins of DNA replication.<sup>23–25</sup> Despite the fact that Pur $\alpha$  and Pur $\beta$  share ~70% sequence identity and exhibit similar ssDNA-binding and helix-destabilizing properties *in vitro*,<sup>26–28</sup> comparative gain-of-function and loss-of-function analyses conducted in transiently transfected fibroblasts and vascular smooth muscle cells point to Pur $\beta$  as the dominant repressor of ACTA2 in these cell types.<sup>29,30</sup> In keeping with its general biological role as a potent repressor of genes that encode contractile proteins, Pur $\beta$  has also been reported to negatively regulate MYH6 and MYH7 in cardiac and skeletal myocytes.<sup>31–33</sup> More recent studies suggest that Pur $\beta$  repressor expression in muscle cells is tightly controlled at the post-transcriptional level by certain muscle-restricted microRNAs to ensure appropriate myofiber composition for sustained cardiac and skeletal muscle performance in response to stress.<sup>34,35</sup>

Apart from hydrodynamic analyses revealing that Pur $\beta$  can reversibly self-associate to form an elongated homodimer in the absence of ssDNA,<sup>36</sup> comparatively little is known about the higher order structural domains in either the Pur $\beta$  monomer or Pur $\beta$  dimer that confer specific and high-affinity interaction with purine-rich elements in ACTA2 or any other target gene. A previous report demonstrated that Pur $\beta$  interacts in a sequential and cooperative manner with the sense strand of the MCAT-containing Pur/Pyr element from mouse ACTA2 to form a high affinity 2:1 Pur $\beta$ /ssDNA complex.<sup>37</sup> While the primary structure of Pur $\beta$  is similar to Pur $\alpha$  in terms of the presence of three distinct regions of internal homology (dubbed PUR repeats I, II, and III),<sup>38</sup> Pur $\beta$  contains several unique intervening sequences with high glycine and proline content that may affect the structural and functional properties of the protein.<sup>26</sup> Importantly, the X-ray crystal structure of a truncated version of *Drosophila melanogaster* (Dm) Pur $\alpha$  (amino acids 40–185) revealed a monomeric Whirly fold-like DNA-binding domain formed by the intramolecular interaction of the first two PUR repeat sequences.<sup>39</sup> On the other hand, we recently identified a core tryptic fragment of Pur $\beta$  (amino acids 29–305) that contains all three PUR repeats, self-associates in the absence of nucleic acid, and retains the ability to interact with the purine-rich strand of the ACTA2-derived MCAT element with high affinity and specificity.<sup>40</sup> In this study, the putative biological role of Pur $\beta$  in suppressing ACTA2 expression and restricting myofibroblast cytodifferentiation was first validated via a stable gene knockdown approach. *In silico* modeling of protein structure coupled with empirical analyses of protein function were then used to delineate the relevant domains in Pur $\beta$  that mediate ACTA2-specific nucleoprotein interaction and repression of the composite MCAT/CAR/GC box enhancer.

## MATERIALS AND METHODS

**Cell Culture and Extraction.** AKR-2B MEF cell lines stably transduced with lentiviral vectors encoding a PURB transcript-specific short hairpin RNA (shRNA) or a scrambled control RNA were generated as described in ref 30. Subcloned cell lines were propagated in McCoy's 5A medium (Gibco/Invitrogen) containing 5% heat-inactivated fetal bovine serum

(FBS) and 10  $\mu$ g/mL blasticidin in a humidified 5% CO<sub>2</sub> incubator and studied at passage number 5 to 15. Phase contrast images of live cells were obtained on a Zeiss Axiovert model 200 inverted microscope equipped with an AxioCam MRm digital camera. Assays used to compare the growth and migratory properties of derived cell lines are detailed in Supporting Information. In timed growth factor treatment experiments, cells were seeded at a fixed density and then switched to serum-free MCDB-402 medium (JRH Biosciences) for 36–48 h. Cells were then treated for 24 h with either 10% FBS or 2.5 ng/mL recombinant human transforming growth factor  $\beta$ 1 (TGF- $\beta$ 1) (R & D Systems) diluted in MCDB-402 medium. Confluent monolayers of growth factor stimulated cells were washed three times with ice-cold phosphate-buffered saline (PBS) and then extracted with 1 $\times$  Reporter Gene Assay Lysis Buffer (Roche Applied Science) supplemented with protease inhibitors, 0.5 mM phenylmethanesulfonyl fluoride and 1  $\mu$ g/mL each of pepstatin A, leupeptin, and aprotinin. Soluble lysates and cell remnants were collected by centrifugation at 15 800g for 10 min at 4 °C. Total protein content in cleared lysates was measured by BCA protein assay (Thermo Scientific) using bovine serum albumin (BSA) as a standard. Insoluble pellets were further extracted with a denaturing solvent consisting of 8 M urea, 100 mM sodium phosphate, 10 mM Tris-Cl, pH 8.0, and protease inhibitors. Denatured lysates were cleared by centrifugation and assayed for protein content as described above.

**Promoter–Reporter Constructs.** Murine ACTA2 promoter–chloramphenicol acetyltransferase reporter constructs (pVSM8-CAT and pVSM4-CAT) have been described elsewhere.<sup>14,30,41</sup> The corresponding ACTA2 promoter–luciferase reporters were constructed as follows. A ~3.6 kb fragment was released from pVSM8-CAT by sequential treatment with *Sph*I, mung bean nuclease, and *Bam*HI. A ~240 bp insert was released from pVSM4-CAT by sequential treatment with *Sall*, mung bean nuclease, and *Bam*HI. Restriction fragments were ligated into *Sma*I/*Bgl*II-digested and alkaline phosphatase-treated pGL3-Basic vector (Promega) to generate pVSM8-Luc and pVSM4-Luc. Following transfection into *Escherichia coli* HB101 cells, ampicillin-resistant clones were selected for propagation and plasmid purification (Roche Applied Science). The fidelity of plasmid constructs was confirmed by restriction enzyme digestion followed by automated DNA sequencing performed by the Vermont Cancer Center DNA Analysis Facility.

**Expression Vectors.** Bacterial and mammalian expression vectors encoding full-length, N-terminal hexahistidine-tagged mouse Pur $\beta$  (pQE30-NHis-Pur $\beta$  and pCI-NHis-Pur $\beta$ ) were described in previous reports.<sup>17,22</sup> Expression plasmids encoding NHis-Pur $\beta$  truncation proteins corresponding to amino acids 41–112 (Pur $\beta$  I), 125–210 (Pur $\beta$  II), 209–303 (Pur $\beta$  III), 41–210 (Pur $\beta$  I–II), 125–303 (Pur $\beta$  II–III), and 41–303 (Pur $\beta$  I–II–III) were constructed following a similar strategy as that outlined in ref 29 and as further detailed in Supporting Information.

**Monoclonal Antibodies.** With the exception of antibody screening assays, all other procedures involved in generating murine and rat monoclonal antibodies (mAbs) recognizing Pur $\alpha$ , Pur $\beta$ , or both were carried out by a commercial vendor (Green Mountain Antibodies). These included rodent immunization, fusion of mouse or rat splenocytes with NS-1 myeloma cells, subcloning of hybridoma cells (two rounds), and *in vitro* production, purification, and isotype/subclass

determination of derived mAbs. The specific antigens used for immunization were keyhole limpet hemocyanin-coupled peptides corresponding to amino acid sequences B42–69, B302–324, and A291–313 of mouse Pur $\beta$  and Pur $\alpha$ , respectively.<sup>22</sup> Animals were immunized with each individual peptide or a combination of all three peptides. The relative affinity and specificity of purified mAbs were evaluated by direct enzyme-linked immunosorbent assay (ELISA) using immobilized peptides or full-length NHis-Pur $\alpha$  or NHis-Pur $\beta$  as described in Supporting Information and shown in Figure S1.

**Computational Modeling of Protein Structure.** A homology model of *Mus musculus* (Mm) Pur $\beta$  was generated based on the structure of *Drosophila melanogaster* (Dm) Pur $\alpha$  repeats I–II (amino acids 40–185) using web-based modeling servers and a bioinformatics approach described previously.<sup>38,39</sup> A pairwise multiple sequence alignment of Mm Pur $\beta$  and Dm Pur $\alpha$  indicating 52% sequence identity was obtained using ClustalW.<sup>42,43</sup> The sequence alignment was submitted to the HHrepID and PSIPRED web servers<sup>44,45</sup> under default parameters to identify repeated sequences and predict secondary structural elements within Pur $\beta$ .<sup>26</sup> To generate a model consistent with these results, the FASTA sequence of Mm Pur $\beta$  was submitted to the I-TASSER web server<sup>46,47</sup> to generate a homology model of Pur $\beta$  repeats I–II using Dm Pur $\alpha$  I–II (3K44) as a template.<sup>39</sup> On the basis of the internal sequence homology of the three Pur $\beta$  repeats, Pur $\beta$  III was independently predicted by SWISS-MODEL<sup>48–50</sup> by threading the sequence of the third Pur $\beta$  repeat onto the structure of Dm Pur $\alpha$  I–II. Predicted intermolecular interaction between two Pur $\beta$  III repeats was modeled by rotating the Mm Pur $\beta$  III repeats of two monomers into an extended conformation and aligning them on Dm Pur $\alpha$  I–II using Coot.<sup>51</sup> Energy minimization of the Pur $\beta$  homodimeric homology model was completed using CNS version 1.2<sup>52,53</sup> to relax close contacts and to regularize local bond and angle geometry. Computationally derived structures were viewed and depicted using PyMOL.<sup>54</sup>

**Recombinant Protein Purification.** Full-length NHis-Pur $\beta$  and selected truncation proteins were expressed in and isolated from *E. coli* JM109 cells using chromatographic methods optimized for each particular recombinant protein as detailed in Supporting Information. NHis-Pur $\beta$ -enriched fractions obtained by metal chelate affinity, heparin affinity, or size exclusion chromatography (SEC) were monitored for purity by sodium dodecyl sulfate–polyacrylamide gel electrophoresis (SDS-PAGE) under reducing conditions and staining with Coomassie Brilliant Blue R-250. Wide range SigmaMarker proteins (Sigma-Aldrich) were used as molecular weight standards. The protein concentration of pooled fractions was determined by absorbance measurement using theoretical molar extinction coefficients at 280 nm of 20 400 M<sup>–1</sup> cm<sup>–1</sup> for full-length NHis-Pur $\beta$  and NHis-Pur $\beta$  I–II–III, 7450 M<sup>–1</sup> cm<sup>–1</sup> for NHis-Pur $\beta$  I–II, and 12 950 M<sup>–1</sup> cm<sup>–1</sup> for NHis-Pur $\beta$  III.<sup>55</sup> Protein preparations were routinely screened to ensure the absence of contaminating nucleic acid as previously described.<sup>36</sup> Protein preparations were also monitored for the presence of nuclease activity by incubating 1.0  $\mu$ M protein stocks with 2  $\mu$ g of either pBLCAT3 plasmid or M13mp18 ssDNA (Bayou Biolabs) for 1 h at 37 °C. The integrity of the DNA substrates was then evaluated by agarose gel electrophoresis. Absence of contaminating nuclease activity in recombinant Pur $\beta$  preparations was established based on

comparison to DNA substrates treated in parallel with 10<sup>–1</sup> to 10<sup>–5</sup> units of DNase I (Invitrogen).

**Calibrated SEC and Circular Dichroism (CD) Spectroscopy.** The quaternary state of purified truncation proteins was determined by SEC on a 1.5  $\times$  100 cm<sup>2</sup> Sephacryl 200 HR column calibrated with molecular weight standards blue dextran, BSA, ovalbumin, carbonic anhydrase, cytochrome C, and DNP aspartate.<sup>36</sup> The folded-ness of recombinant proteins was assessed by CD spectroscopy. All proteins were analyzed on a Jasco model 815 spectrometer after dialysis into buffer consisting of 50 mM Tris-Cl, pH 7.5, 300 mM NaCl, 0.5 mM EDTA, and 0.5 mM tris(2-carboxyethyl)phosphine hydrochloride (TCEP). Multiple wavelength scans were recorded at 1 nm intervals from 195 to 280 nm on 5.0  $\mu$ M protein solutions in a 1 mm cuvette at 25 °C. Raw CD data were analyzed as previously described.<sup>40</sup>

**Single-Stranded DNA-Binding Assays.** Direct or competitive colorimetric microplate-based assays were conducted with purified proteins and a 3' biotinylated ssDNA probe corresponding to the purine-rich strand of the murine ACTA2 5'-flanking sequence from –195 to –164 (PE32-bF) as previously described.<sup>40,56</sup> In the direct ssDNA-binding format, solid-phase Pur $\beta$ –PE32-bF complexes were detected by ELISA using primary rabbit antibodies directed against amino acids 210–229 or 302–324 of mouse Pur $\beta$ <sup>22</sup> or the NHis tag (His probe H-15 from Santa Cruz Biotechnology, Inc., or anti-6-His from Bethyl Laboratories, Inc.). In the competitive binding format, solid-phase nucleoprotein complexes were detected with ExtraAvidin–peroxidase (Sigma-Aldrich). Log protein concentration versus absorbance data sets were fit to four-parameter variable-slope equations to determine EC<sub>50</sub> or IC<sub>50</sub> values depending on the format of the assay (Prism 5, Version 5.04, Graphpad Software, Inc.).

**Protein–Protein Interaction Assay.** Protein–protein interaction was assessed in an ELISA format using microtiter wells (Costar EIA/RIA 96 well plate, certified high binding, Corning Inc.) coated with 200 nM NHis-Pur $\beta$  or selected truncation proteins as previously described.<sup>30,56</sup> Nuclear extracts prepared from exponentially growing AKR-2B MEFs served as a source of protein binding partners of Pur $\beta$ .<sup>57</sup> The primary antibodies used for detection of solid-phase protein–protein complexes included rabbit anti-mouse Pur $\alpha$  291–313,<sup>22</sup> rabbit anti-mouse YB-1 (MSY1) 242–269,<sup>22</sup> and rabbit anti-mouse TEF1 1–15.<sup>17</sup> Commercial rabbit polyclonal antibodies against SRF (G-20), Sp1 (H-225 and PEP-2), and Sp3 (D-20) were from Santa Cruz Biotechnology, Inc.

**Transient Transfection Assay.** AKR-2B MEFs were seeded into six well plates at 4.0  $\times$  10<sup>4</sup> cells per well in McCoy's 5A medium with 5% FBS. Primary mouse aortic outgrowth smooth muscle cells (AoSMCs)<sup>30</sup> were seeded at 2.5  $\times$  10<sup>4</sup> cells per well in DMEM with 10% FBS. After an overnight incubation at 37 °C in a 5% (MEFs) or 10% (AoSMCs) CO<sub>2</sub> incubator, adherent cells were transfected with 2  $\mu$ g of total DNA using jetPEI reagent (PolyPlus-transfection) at a ratio of 1.5  $\mu$ L per  $\mu$ g of DNA. Transfection solutions typically contained 0.9  $\mu$ g of pVSMP8- or pVSMP4-CAT or luciferase reporters, 0.1  $\mu$ g of pSV40- $\beta$ -Gal control reporter, and 1.0  $\mu$ g of expression plasmid. After 48 h incubation at 37 °C, cells were washed with PBS and then extracted with 1 $\times$  Passive Lysis Buffer (Promega) supplemented with protease inhibitors. Total protein content was determined by BCA or Bradford assay, and individual reporters were measured with the use of a CAT or  $\beta$ -Gal ELISA kit (Roche Applied Science),



Luciferase Assay System (Promega), or *ortho*-nitrophenyl- $\beta$ -galactoside chromogenic substrate assay. Numerical data sets were subjected to one-way analysis of variance and Tukey's multiple comparison test with significance set at  $p < 0.05$  (Prism 5, Version 5.04, Graphpad Software, Inc.). In some instances, transfected cells were processed by sequential extraction using a subcellular protein fractionation kit as directed by the manufacturer (Thermo Scientific).

**Immunoblotting.** Samples were prepared for SDS-PAGE by dilution of concentrated cell lysates into 6 $\times$  sample preparation buffer (120 mM Tris-Cl, pH 6.8, 3% w/v SDS, 30% v/v glycerol, 0.03% w/v bromophenol blue). For less concentrated cell lysates, soluble protein was precipitated by adding 5 volumes of ice-cold ethanol to 1 volume of cell lysate and incubating for at least 1 h at  $-20^{\circ}\text{C}$ . Precipitated protein was collected by centrifugation and dissolved in 1 $\times$  SDS-PAGE loading buffer. Samples were supplemented with 5% v/v 2-mercaptoethanol, heated for 3–5 min at  $100^{\circ}\text{C}$ , and subjected to slab gel electrophoresis on 10%, 12%, or 15% w/v acrylamide/bisacrylamide (29:1) mini-gels or 4–20% precast gradient gels (Lonza). Molecular weight standards were run in parallel on each gel (BenchMark Prestained Protein Ladder, Invitrogen). Proteins were then electrotransferred to Immobilon-P or Immobilon-PSQ polyvinylidene difluoride membrane (Millipore) in 25 mM Trizma base, 192 mM glycine, 20% v/v methanol at 125 V for 90 min at  $4^{\circ}\text{C}$ . Transblots were probed with selected antibodies as described in ref 22. Primary and secondary antibodies used are listed in Supporting Information.

## RESULTS

**Derivation of Pur $\beta$  Knockdown MEFs.** To assess the phenotypic consequence of Pur $\beta$  loss-of-function in a multipotent mesenchymal cell type, a lentiviral shRNA expression system was used to stably transduce AKR-2B MEFs owing to their high steady-state levels of Pur $\alpha$  and Pur $\beta$  and sensitivity to inducers of myofibroblast differentiation.<sup>20,22,58</sup> As shown in Figure 1A, specific knockdown of Pur $\beta$  (faster migrating band of doublet) was confirmed in two independently derived blasticidin-resistant cell lines by Western blotting with the use of a newly developed rat monoclonal antibody directed against a conserved PUR repeat I sequence present in both Pur $\alpha$  and Pur $\beta$  (specifically, amino acids 42–69 of Pur $\beta$ ). Importantly, Pur $\alpha$  expression (slower migrating band of doublet) was not altered in either Pur $\beta$ -only knockdown cell line ( $\beta$ I-B4 and  $\beta$ I-G7) compared with control cells transduced with scrambled RNA ( $\beta$ S-E6). For the purpose of comparison, extract from a serendipitously derived cell line deficient in Pur $\alpha$  expression ( $\beta$ I-F3) was included on the gel to highlight differences in the electrophoretic mobility of bands corresponding to Pur $\alpha$  and Pur $\beta$ . To quantify relative differences in Pur $\beta$  expression, a functional ELISA was used to measure Pur $\beta$  ssDNA-binding activity in soluble extracts of each cell line (Figure 1B). In keeping with the results of Western blotting, Pur $\beta$  ssDNA-binding activity was reduced by 2.5–2.7-fold in the  $\beta$ I-B4 and  $\beta$ I-G7 cells in comparison to the  $\beta$ S-E6 control cell line. Consistent with a dominant Pur $\alpha$  loss-of-function phenotype,<sup>59</sup> the Pur $\alpha$ -deficient  $\beta$ I-F3 cell line exhibited a markedly enhanced rate of cell growth relative to Pur $\beta$ -only knockdown and scrambled control cell lines and was thus excluded from detailed study (Figure S2, Supporting Information).

**Phenotypic Properties of Pur $\beta$  Knockdown MEFs.** Analysis of growing MEF cell lines by light microscopy revealed that Pur $\beta$ -only knockdown cells adopt a more elongated

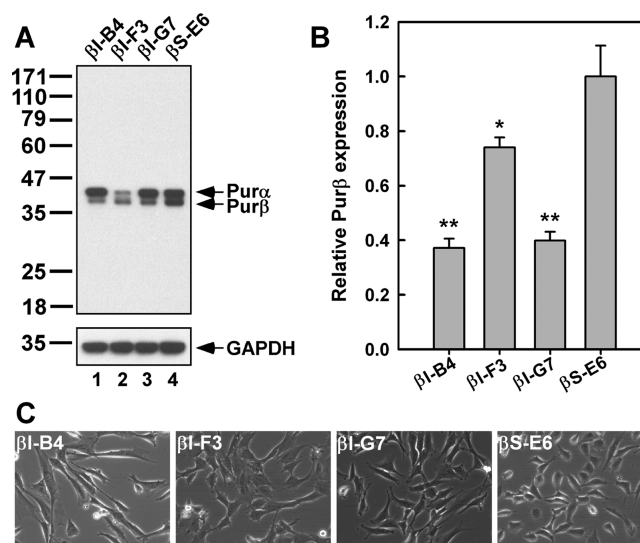


**Figure 1.** Validation of constitutive Pur $\beta$  knockdown in MEFs. (A) Immunoblotting of whole cell extracts (10  $\mu$ g of protein per lane) from the indicated MEF cell lines was conducted with a mAb (rat anti-Pur $\beta$  42–69 clone 3C3.6C1) directed against a conserved PUR repeat I epitope present in both Pur $\alpha$  (slower migrating band) and Pur $\beta$  (faster migrating band). The Pur $\alpha$ / $\beta$  blot was reprobed with a GAPDH mAb to confirm equivalent protein loading.  $\beta$ I-B4 and  $\beta$ I-G7 (lanes 1 and 3) are two distinct clonal cell lines stably expressing a Pur $\beta$  shRNA, while  $\beta$ S-E6 is a control cell line stably expressing a scrambled RNA (lane 4). For the purpose of comparison,  $\beta$ I-F3 (lane 2) is a serendipitously isolated cell line deficient in Pur $\alpha$  expression. Lines and numbers on the left side designate the relative position and size (in kDa) of prestained protein markers. (B) Quantification of functional Pur $\beta$  protein in extracts from the indicated MEF cell lines by ssDNA-binding ELISA. Bars show Pur $\beta$  expression relative to  $\beta$ S-E6 control cells (mean  $\pm$  SEM,  $n = 4$ ). \*,  $p < 0.05$ , \*\*,  $p < 0.01$  compared with  $\beta$ S-E6. (C) Phase contrast micrographs of subconfluent cultures of the indicated MEF cell lines viewed through a 20 $\times$  objective.

spindle-like morphology in comparison to control cells expressing scrambled RNA (Figure 1C). A similar but less dramatic change in morphology is evident in cells co-deficient in Pur $\alpha$ . These morphological differences were readily apparent in confluent cell monolayers as well (Figure S3, Supporting Information). To investigate the physical basis for these changes in cell shape, the expression of cytoskeletal actin proteins was assessed by immunoblotting of detergent-soluble and detergent-insoluble lysates prepared from serum- or TGF- $\beta$ 1-stimulated MEF cell lines. In serum-stimulated cells, the soluble G-form of SM $\alpha$ A was the predominant actin isoform exhibiting enhanced expression in concert with Pur $\beta$  knockdown, although a slight increase in  $\beta$ -actin expression was detected as well (Figure 2A). Consistent with sensitization to TGF- $\beta$ 1-driven myofibroblast cytodifferentiation, a corresponding increase in both G- and F-form SM $\alpha$ A, but not  $\beta$ -actin, was seen in Pur $\beta$  knockdown MEFs relative to the control cell line treated with TGF- $\beta$ 1 (Figure 2B). Pur $\beta$  deficiency, however, did not promote acquisition of a smooth muscle cell-like protein expression pattern because other markers of smooth muscle differentiation including smooth muscle myosin and SM22 $\alpha$ /transgelin were not detected by immunoblotting of either control or Pur $\beta$  knockdown MEFs (data not shown). To determine whether increased expression of SM $\alpha$ A protein correlated with de-repression of ACTA2 transcription, transient

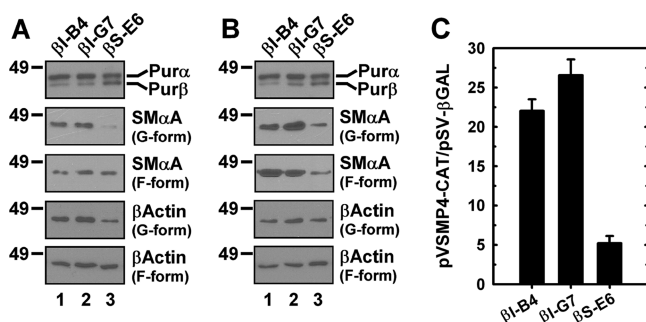


**Figure 2.** Knockdown of Purβ enhances SMαA expression in growth factor-stimulated MEFs. (A, B) Immunoblotting of cell extracts prepared from Purβ knockdown (lanes 1 and 2) and control (lane 3) MEFs stimulated with either serum (A) or TGF-β1 (B) was conducted with mAbs against Purα/β, SMαA, or β-actin. Purα/β (10 μg protein/lane) and G-form actin (0.5 μg protein/lane) were detected in detergent-soluble cell lysates. F-form actins were detected in detergent-insoluble cell remnants dissolved in 8 M urea (0.2 μg of protein loaded per lane). (C) The indicated MEF cell lines were transiently transfected with a combination of pVSMP4-CAT and pSV-βgal promoter-reporter constructs. Cell extracts were prepared 48 h later, and reporter enzymes were quantified by ELISA. Bars show the ratio of CAT to β-gal measured in each cell line normalized for total protein (mean ± SEM).

transfection assays were conducted using a minimal MCAT- and CArG-dependent ACTA2 enhancer–promoter construct. As shown in Figure 2C, ACTA2-driven reporter expression was significantly increased in both Purβ knockdown cell lines in comparison to control cells implying that loss of Purβ repressor function is necessary and sufficient to promote ACTA2

expression and myofibroblast differentiation in MEFs. In keeping with the known motility-restrictive properties of SMαA-containing myofilaments in cultured fibroblasts,<sup>60</sup> Purβ knockdown MEFs also demonstrated a modest reduction in chemotactic migration toward serum growth factors as measured by Boyden chamber assay (Figure S4, Supporting Information).

**Homology Modeling of Purβ Tertiary and Quaternary Structure.** To explore the physical basis for Purβ-mediated repression of ACTA2 transcription, we first set out to computationally model the higher order structure of Purβ based on (1) sequence homology with other members of the purine-rich element binding protein family and (2) the known X-ray crystal structure of *Dm* Purα 40–185. Primary sequence analysis of *Mm* Purβ using selected homology detection and structure prediction algorithms indicated that Purβ possesses the same linear arrangement of PUR repeat modules (designated I, II, and III) as originally described in Purα<sup>38,39</sup> (Figure 3A). The sequences encoding *Mm* Purα and *Mm* Purβ were threaded on the X-ray crystal structure of *Dm* Purα residues 40–185 (3K44) using SWISS-MODEL to assess the overall homology of the intramolecular PUR domain formed by PUR repeats I and II of each protein. As expected, the major differences were restricted to putative loop regions connecting the individual PUR I and II repeats while the β-strand and α-helix forming sequences were virtually superimposable (Figure S5, Supporting Information). To create a hypothetical structure of the full-length Purβ monomer, PUR repeat III was independently modeled using SWISS-MODEL, and the tertiary structure of the entire protein was constructed on the basis of an I-TASSER generated template (Figure 3B). Like PUR

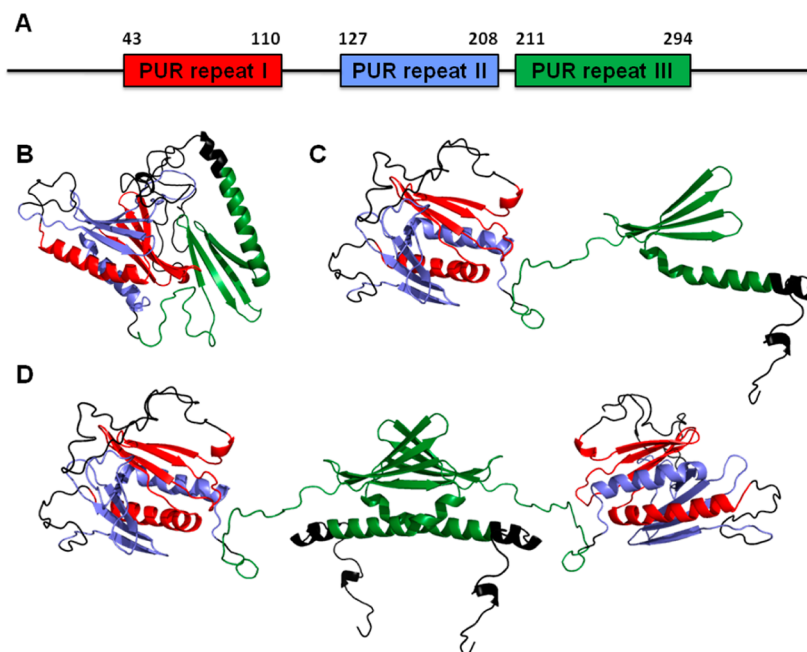


**Figure 3.** Computational models of *Mm* Purβ monomer and dimer. (A) The primary sequence of the 324 amino acid *Mm* Purβ was analyzed by HHrepID. Predicted regions corresponding to PUR repeats I, II, and III are highlighted in red, blue, and green, respectively. Numbers refer to amino acid positions. Intervening elements and N- and C-terminal regions are shown as black lines. (B) Web servers (I-TASSER and SWISS-MODEL) were used to generate a homology model of the Purβ monomer. In this hypothetical model, PUR repeat III (green) is in a closed conformation relative to the intramolecular PUR domain formed by PUR repeats I (red) and II (blue). (C) A model of the Purβ monomer in an extended conformation was generated by rotating the PUR repeat III away from the intramolecular domain formed by PUR repeats I and II. (D) A model of the Purβ dimer was created by aligning the PUR III repeats of two Purβ monomers in such a way as to form an intermolecular PUR domain that is predicted to mediate protein self-association.

repeats I and II, PUR repeat III is predicted to possess similar  $\beta\beta\beta\alpha$  topology. However, a putative random coil-forming region located between PUR repeats II and III may impart some degree of flexibility as to the position of PUR repeat III relative to the intramolecular domain formed by PUR repeats I and II (Figure 3C). Consequently, dimerization may occur via formation of an intermolecular PUR domain composed of two self-associating PUR III repeats from two Pur $\beta$  monomers (Figure 3D).

**Structural Analysis of Computationally Derived Pur $\beta$  Subdomains.** To test the models in Figure 3, a series of cDNAs were engineered to encode NHis-tagged Pur $\beta$  truncation proteins corresponding to individual PUR repeat modules (Pur $\beta$  I, Pur $\beta$  II, Pur $\beta$  III) or selected combinations thereof (Pur $\beta$  I–II, Pur $\beta$  II–III, Pur $\beta$  I–II–III). The utility of recombinant NHis-Pur $\beta$  as a reliable experimental surrogate for the native protein expressed in mammalian cells has been documented in previous studies.<sup>29,37,56</sup> Sequence validated bacterial expression plasmids were transformed into *E. coli* cells, and recombinant truncation proteins were produced for trial purification under both native and denaturing conditions. While metal chelate affinity enrichment of each Pur $\beta$  truncation protein was possible under harsh denaturing conditions (data not shown), only Pur $\beta$  I–II–III (residues 41–303), Pur $\beta$  I–II (residues 41–210), and Pur $\beta$  III (residues 209–303) were amenable to purification in nondenaturing solvents (Figure S6, Supporting Information) and were found to exhibit CD spectra consistent with well-folded polypeptides (Figure S7, Supporting Information). Hence, it appeared that Pur $\beta$  I (residues 41–112), Pur $\beta$  II (residues 125–210), and Pur $\beta$  II–III (residues 125–303) were intrinsically unstable or misfolded when expressed in *E. coli*. This observation is consistent with the putative requirement for intramolecular association of PUR repeats I and II or intermolecular association of two PUR III repeats to form a stably folded subdomain (Figure 3). To confirm the predicted quaternary state of each isolated truncation protein, calibrated SEC was performed using loading concentrations well in excess of the reported  $K_d$  for the full-length Pur $\beta$  dimer.<sup>36</sup> As shown in Figure 4A,B, Pur $\beta$  I–II–III eluted as a ~64 kDa dimer, while Pur $\beta$  I–II resolved as a ~18 kDa monomer. In agreement with its predicted role in mediating self-association, Pur $\beta$  III eluted as a ~17 kDa dimer (Figure 4C).

**ACTA2 Repressor Activity of Pur $\beta$  Subdomains.** To assess the functional role of each putative Pur $\beta$  subdomain in ACTA2 repression, transient cotransfection assays were performed in MEFs and primary mouse AoSMCs using a full-length ACTA2 construct (–1070 to +2582, VSMP8-Luc) as well as a minimal MCAT/CAR/GC box-dependent enhancer (–146 to +46, VSMP4-Luc) as specific transcriptional targets of Pur $\beta$ .<sup>30</sup> As shown in Figure 5B, full-length Pur $\beta$  and the core I–II–III construct demonstrated comparable repressor activity toward both ACTA2 reporters in MEFs. Importantly, Pur $\beta$  I–II was the only other truncation protein to exhibit statistically significant repressor activity. Pur $\beta$  III alone showed no inhibitory activity while Pur $\beta$  II–III was only weakly repressive. In agreement with *E. coli* expression and purification studies, immunoblotting of nondenatured MEF lysates indicated stable expression of full-length Pur $\beta$ , Pur $\beta$  I–II–III, Pur $\beta$  I–II, and Pur $\beta$  III (Figure 5C). However, Pur $\beta$  I, Pur $\beta$  II, and Pur $\beta$  II–III were either not readily detected or only seen after extracting detergent-insoluble cell remnants with a denaturing solvent (Figure 5D), again pointing to the intrinsic instability or

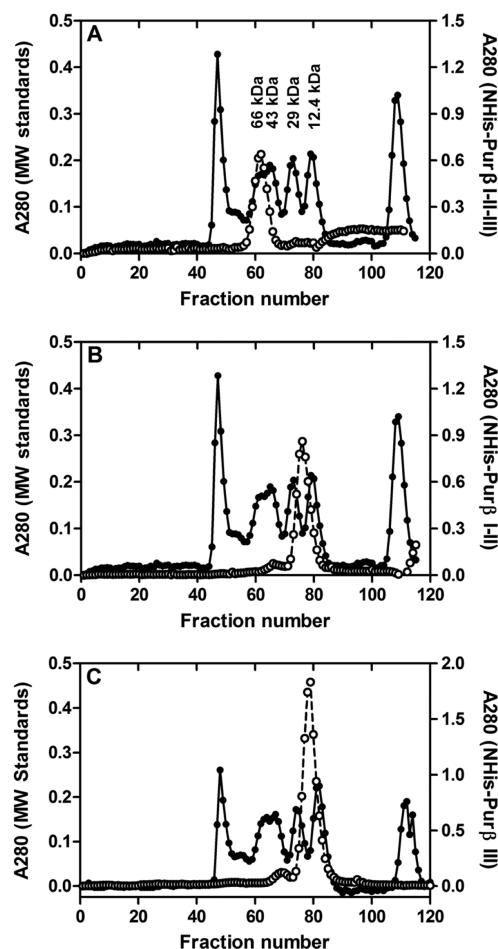


**Figure 4.** Quaternary structure of isolated Pur $\beta$  subdomains. (A–C) Calibrated SEC was conducted on preparations of Pur $\beta$  I–II–III (A), Pur $\beta$  I–II (B), and Pur $\beta$  III (C) at loading concentrations in excess of 10  $\mu$ M (○). The elution profile of a mixture of molecular weight standards is shown for comparison (●). Numbers in panel A indicate the apparent molecular weights of the four globular protein standards used in generating a standard curve to calculate the size of the Pur $\beta$  species eluting in the peak fractions.

misfolding of these truncation mutants. Essentially identical results were obtained in cotransfection studies conducted with primary AoSMCs (Figure S8, Supporting Information) corroborating the conclusion that the relative ACTA2 repressor activity of the stably expressed truncation proteins is Pur $\beta$  I–II–III > Pur $\beta$  I–II  $\gg$  Pur $\beta$  II–III or Pur $\beta$  III. Titration studies conducted in AKR-2B MEFs using a fixed amount of VSMP8 reporter and varying amounts of expression plasmid confirmed that Pur $\beta$  I–II–III and Pur $\beta$  I–II are quantitatively distinct in terms of their ACTA2 repressor activity (Figure 6).

**Cis-Element Binding Properties of Pur $\beta$  Subdomains.** To assess whether the relative ACTA2 repressor activity of each Pur $\beta$  truncation protein correlated with differences in their affinity or specificity for target sites in the ACTA2 promoter, colorimetric microplate-based assays were used to compare the ssDNA-binding properties of Pur $\beta$  I–II–III, Pur $\beta$  I–II, and Pur $\beta$  III to full-length Pur $\beta$ . The purine-rich sense strand of the 5' ACTA2 Pur/Pyr element containing a consensus core MCAT motif (*italicized*) (GGGAGCAGAACAGAGGAATG-CAGTGGAAAGAGA, PE32-F) was chosen as a probe because it has multiple interacting binding sites (underlined) that permit formation of a high-affinity (macroscopic  $K_d \approx 0.3$  nM)



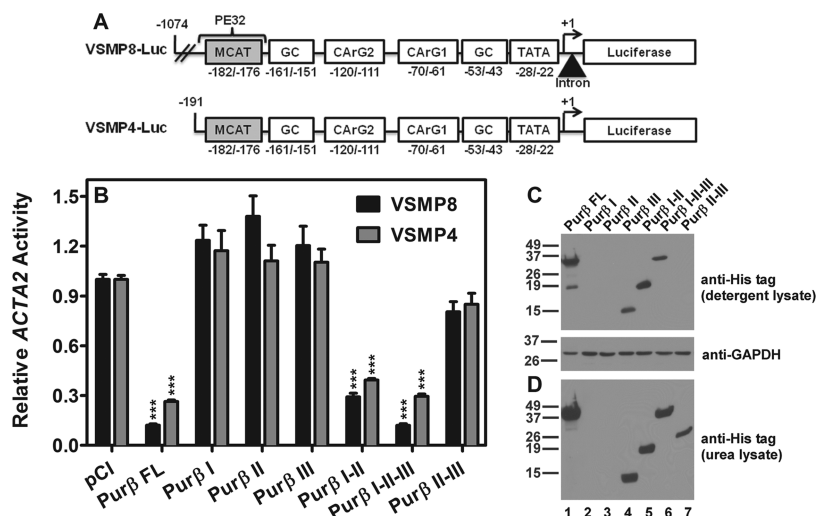


**Figure 5.** ACTA2 repressor activity of Purβ truncation proteins expressed in AKR-2B MEFs. (A) Schematic representation of the full-length (VSMP8-Luc) and truncated (VSMP4-Luc) ACTA2 promoter–reporter constructs used to assess Purβ repressor function. PE32 designates the Purβ recognition sequence containing an MCAT motif. (B) Subconfluent AKR-2B MEFs were transiently cotransfected with ACTA2 luciferase reporters and expression vectors encoding the indicated Purβ proteins. After 48 h, cell lysates were prepared and assayed for luciferase activity and total protein. Bars show total protein-corrected luciferase values normalized to the pCI control (defined as 1) for each reporter (mean ± SEM,  $n = 9$ ). \*\*\*,  $p < 0.001$  compared with pCI control for VSMP8 (black bars) or VSMP4 (gray bars). (C) Western blotting of detergent-soluble lysates (15 μg of protein per lane) of transfected cells was performed with a mAb recognizing the N-terminal His epitope tag present on each Purβ construct. The anti-His tag blot was reprobed with a GAPDH mAb as a loading control. (D) Western blotting of urea-denatured lysates (15 μg of protein per lane) of detergent-insoluble cell remnants was conducted with the His tag mAb. (C, D) In both immunoblots, lysates were resolved on a 15% polyacrylamide gel. Lines and numbers on the left side designate the relative position and size (in kDa) of prestained protein markers. FL, full-length.

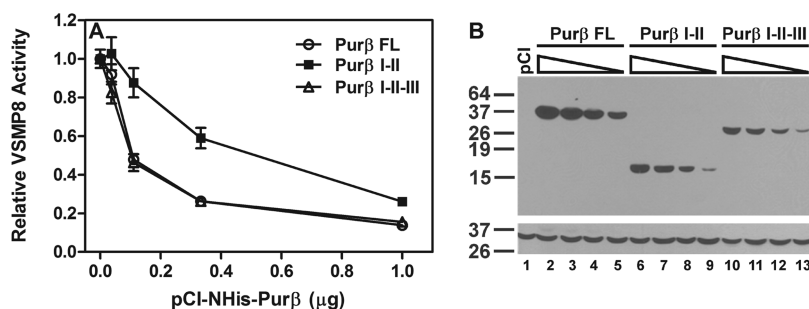


**Figure 6.** Relative ACTA2 repressor activity of Purβ truncation proteins expressed in AKR-2B MEFs. (A) AKR-2B MEFs were transiently cotransfected with a fixed amount of ACTA2 luciferase reporter (VSMP8) and varying amounts of expression vector encoding the indicated Purβ proteins. After 48 h, cell lysates were prepared and assayed for luciferase activity and total protein. Symbols show total protein-corrected luciferase values normalized to the pCI control (mean ± SEM,  $n = 6$ ). (B) Immunoblots of transfected cell lysates (15 μg of protein per lane) with a His tag mAb (top panel) followed by a GAPDH mAb (lower panel). Lines and numbers on the left side designate the relative position and size (in kDa) of prestained protein markers. FL, full-length.

2:1 Purβ/ssDNA complex.<sup>37</sup> Initially, a titration experiment was performed to identify a minimal concentration of 3' biotinylated PE32-F probe necessary to detect the interaction of each Purβ truncation protein by ELISA. Surprisingly, stable formation of Purβ I–II nucleoprotein complexes required a markedly higher concentration of ssDNA implying a significant difference in binding affinity of the monomeric subdomain relative to full-length Purβ, Purβ I–II–III, and Purβ III (Figure S9A, Supporting Information). Titration assays conducted with a limiting concentration of PE32-bF (0.5 nM) highlighted the striking differences in the apparent ssDNA-binding affinity of the individual subdomains, Purβ III ( $EC_{50} = 1.80 \pm 0.74$  nM,  $n = 4$ ) and Purβ I–II ( $EC_{50} > 100$  nM), relative to the full-length protein ( $EC_{50} = 0.16 \pm 0.05$  nM,  $n = 4$ ) and Purβ I–II–III ( $EC_{50} = 0.22 \pm 0.05$  nM,  $n = 4$ ) (Figure 7A,B). Consistent with a functional distinction between the separated dimerization and intramolecular subdomains, competition assays revealed that

Purβ III ( $IC_{50} = 46 \pm 15$  nM,  $n = 3$ ) and Purβ I–II ( $IC_{50} > 1000$  nM) were much less effective than the composite Purβ I–II–III construct ( $IC_{50} = 1.0 \pm 0.3$  nM,  $n = 5$ ) or the full-length protein ( $IC_{50} = 1.2 \pm 0.2$  nM,  $n = 5$ ) at inhibiting the interaction of 0.5 nM PE32-bF with immobilized Purβ (Figure 7C). Despite these substantial differences in apparent ssDNA-binding affinity, the isolated Purβ III and Purβ I–II subdomains retained similar binding site specificity as demonstrated by their reduced interaction with mutant versions of PE32-bF containing heptathymidylate substitutions (T7) in place of 5' or 3' PUR or internal MCAT motifs (Figure 7D and Figure S9B, Supporting Information).

**Trans-Acting Factor Binding Properties of Purβ Subdomains.** To ascertain whether the isolated subdomains exhibited similar protein binding properties as full-length Purβ, an ELISA-based profiling assay was conducted using nuclear extract from AKR-2B MEFs as a natural source of potential

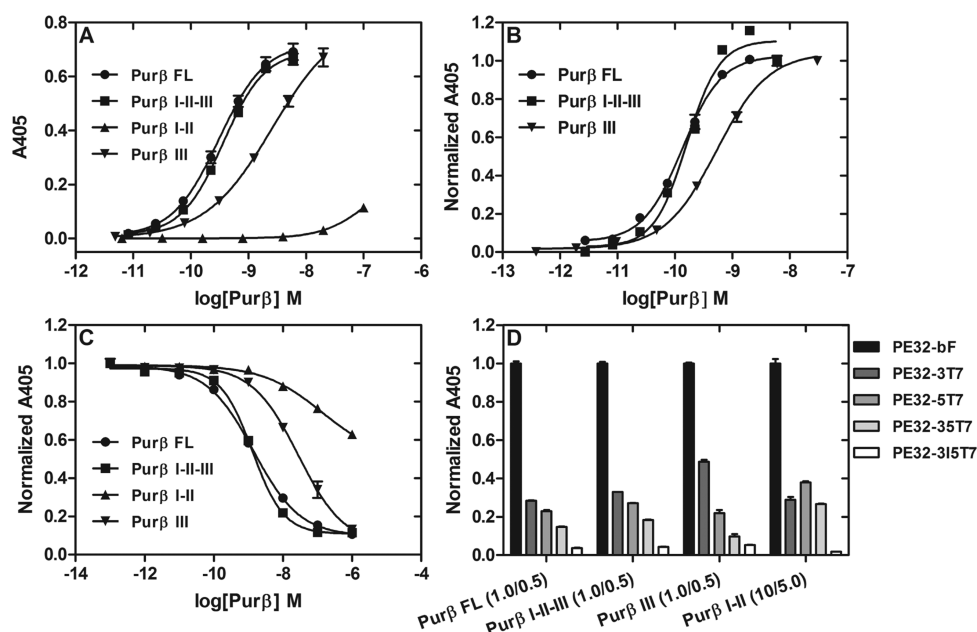


**Figure 7.** The relative affinity and specificity of Pur $\beta$  truncation proteins for ssDNA. (A, B) Varying concentrations of the indicated NHis-Pur $\beta$  proteins were incubated with 0.5 nM biotinylated mouse ACTA2-derived ssDNA probe (PE32-bF) immobilized on StreptaWells. (A) Solid-phase nucleoprotein complexes were detected by ELISA using a primary antibody recognizing the NHis tag. Absorbance values at 405 nm (A405) were corrected for nonspecific binding by subtracting the signal generated in wells with no DNA. (B) Solid-phase nucleoprotein complexes were detected by ELISA using a primary antibody directed against amino acids 210–229 of Pur $\beta$ . A405 values were corrected for nonspecific binding and normalized to the absorbance obtained at the maximum concentration of each protein tested (defined as 1). (C) Varying concentrations of fluid-phase Pur $\beta$  proteins were incubated with a fixed concentration of PE32-bF (0.5 nM) in microtiter wells precoated with full-length Pur $\beta$  (20 nM). Solid-phase nucleoprotein complexes were detected by colorimetric assay using an avidin–peroxidase conjugate. A405 values were normalized to the maximum absorbance obtained in the absence of any competitor. (A, B, C) Data points were fit to a four-parameter equation to determine an EC<sub>50</sub> (A, B) or IC<sub>50</sub> (C) for each protein. A representative experiment is shown in each panel. (D) A fixed concentration of Pur $\beta$  protein was incubated with wild-type or mutant ssDNA probes immobilized on StreptaWells. The ratio of Pur $\beta$  to ssDNA tested (nM/nM) is indicated in parentheses. Solid-phase nucleoprotein complexes were detected by ELISA with a primary His tag antibody. A405 values were corrected for nonspecific binding and normalized to the absorbance obtained for each protein binding to the wild-type probe (defined as 1). FL, full-length.

Pur $\beta$  interaction partners. Recombinant Pur $\beta$  proteins were immobilized on microtiter wells at a saturating coating concentration (200 nM) and then assayed for their ability to capture specific transcription factors implicated in ACTA2 activation or repression. Consistent with previous findings,<sup>30,56</sup> full-length Pur $\beta$  demonstrated preferential interaction with its co-repressor partner MSY1 relative to other factors screened using this assay format (Figure 8). Interestingly, Pur $\beta$  I–II–III exhibited an even greater binding capacity for MSY1, while the isolated Pur $\beta$  I–II and Pur $\beta$  III subdomains displayed markedly reduced interaction with MSY1. In contrast, Pur $\beta$  I–II showed a clear preference for interaction with the ACTA2 transactivator Sp3, while Pur $\beta$  III exhibited little or no Sp3 binding activity. Essentially identical results were obtained using nuclear extract diluted in binding buffer supplemented with reducing agent (Figure S10, Supporting Information). This was done to ensure that the differences observed in the binding properties of individual Pur $\beta$  truncation proteins were not attributable to anomalous protein oxidation.

## DISCUSSION

The transient differentiation of stromal fibroblasts to contractile, SM $\alpha$ A-expressing myofibroblasts is an essential and tightly regulated component of the wound healing process. Conversely, sustained stromal myofibroblast activation is pathologic because it often promotes aberrant tissue remodeling.<sup>61</sup> Because SM $\alpha$ A expression is a biochemical hallmark of the myofibroblast phenotype, a better understanding of the

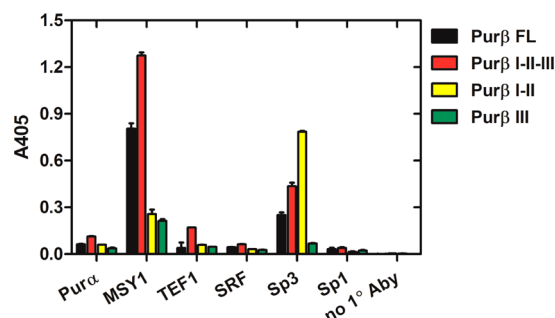


**Figure 8.** Relative binding of AKR-2B MEF-derived transcription factors to purified NHis-Pur $\beta$  proteins. Microtiter wells coated with equivalent concentrations of the indicated Pur $\beta$  proteins (200 nM) were incubated with a fixed amount of nuclear protein (250  $\mu$ g/mL) diluted in binding buffer. Solid-phase protein–protein complexes were detected by ELISA using primary rabbit polyclonal antibodies recognizing Pur $\alpha$ , MSY1, TEF1, SRF, Sp3, or Sp1. Absorbance values at 405 nm generated with each transcription factor antibody were corrected for nonspecific antibody binding to Pur $\beta$  coated wells in the absence of nuclear extract. Signal generated in Pur $\beta$ -coated wells incubated with nuclear extract and probed with the secondary antibody only (no 1° Aby) is shown as a background control. FL, full-length.

regulatory factors that mediate ACTA2 transcription and translation in fibroblasts may reveal novel targets for therapeutic intervention to limit destructive fibrocontractile remodeling associated with scarring, fibrosis, and tumor



progression. Among the factors implicated in *ACTA2* regulation in fibroblasts, *Purα* and *Purβ* are unique in that they apparently repress gene transcription by forming nucleoprotein complexes with purine-rich ssDNA in such a way as to block *trans*-activator recognition of cognate double-stranded binding sites within the composite MCAT/CARG/GC box enhancer.<sup>16,17,30,62</sup>

In view of a growing body of evidence suggesting that *Purβ* may play a central role in repressing genes encoding muscle-restricted isoforms of actin and myosin in both myogenic and nonmyogenic cell types,<sup>31–35</sup> we initially sought to confirm that deficiency of *Purβ* in MEFs would necessarily promote the acquisition of a myofibroblast phenotype *in vitro*. To do so, we transduced MEFs using a lentivirus-based shRNA transgene delivery system to knockdown the expression of *Purβ* in a specific, stable, and constitutive manner. Analyses of two independently derived cell lines showed that a relatively modest decrease in *Purβ* expression (~60–70% knockdown) was sufficient to switch cells to a myofibroblast-like phenotype as exemplified by characteristic changes in cell morphology, *SMAα* expression, TGF- $\beta$ 1 inducibility, and chemotactic migration (Figures 1 and 2; Figures S3 and S4, Supporting Information). Importantly, these changes occurred in the absence of any substantive effect on cell growth suggesting that *Purβ* does not participate in the direct regulation of cell cycling as has been reported for *Purα*.<sup>63–68</sup>

To better understand the structural basis for *Purβ*-mediated repression of *ACTA2*, we employed web-based homology modeling servers to generate computational models of the *Purβ* monomer and dimer based on the known X-ray crystal structure of *Dm Purα* residues 40–185.<sup>39</sup> As previously described for *Purα*,<sup>38</sup> the HHrepID web server identified three regions of internal sequence homology termed PUR repeats I, II, and III (Figure 3). Homology modeling suggested that each PUR repeat is similarly structured with respect to the arrangement of four  $\beta$ -stands and one  $\alpha$ -helix. By analogy to the tertiary structure of *Dm Purα* I–II, *Mm Purβ* I–II is predicted to fold in such a way as to form an intramolecular PUR domain with features resembling a Whirly class-like DNA-binding fold.<sup>39</sup> Although the PUR III repeat of *Purβ* is also predicted to adopt  $\beta\beta\beta\beta\alpha$  topology, the  $\alpha$ -helical region is substantially longer than those in PUR repeats I and II owing to the presence of the so-called “psycho” motif spanning residues 264–291.<sup>26</sup> This sequence is predicted to form an extended amphipathic  $\alpha$ -helix, which may facilitate protein–protein interaction. In one hypothetical model of the *Purβ* monomer, the PUR III repeat is depicted as packing against the PUR I–II intramolecular domain (Figure 3B). However, previous hydrodynamic studies showed that full-length *Purβ* reversibly self-associates to form an elongated homodimer.<sup>36</sup> Therefore, we speculated that the glycine-rich sequence spanning residues 210–229 may impart some degree of internal flexibility allowing the PUR III repeat region to extend away from I–II (Figure 3C). The interaction of two PUR III repeats to form an intermolecular PUR domain would necessarily give rise to an elongated *Purβ* homodimer composed of three distinct modules (Figure 3D).

Based on these deduced homology models, we created a set of expression vectors encoding His-tagged *Purβ* truncation proteins containing single or selected combinations of PUR repeats I, II, and III. Trial purifications from *E. coli* indicated that stable expression and folding of *Purβ* requires the formation of specific intra- or intermolecular subdomains. For

example, *Purβ* I, *Purβ* II, and *Purβ* II–III constructs were poorly expressed or only detectable in denatured lysates. Conversely, full-length *Purβ*, *Purβ* I–II–III, *Purβ* I–II, and *Purβ* III were each highly expressed and readily purified under nondenaturing conditions. Moreover, their respective CD spectra were indicative of well-folded polypeptides. The results of calibrated SEC analysis confirmed the predicted quaternary state of each purified truncation protein and indicated that PUR repeat III constitutes the dimerization domain of *Purβ* (Figure 4). These findings are entirely consistent with the reported quaternary structures of *Dm Purα* I–II and *Dm Purα* I–II–III.<sup>39</sup> Although the *Purα* homodimer has been proposed to adopt a Z-like shape based on results of small angle-X-ray scattering,<sup>39</sup> the exact orientation and relation of the intra- and intermolecular subdomains in the *Purβ* homodimer is currently unknown.

To evaluate the capacity of each *Purβ* truncation protein to repress *ACTA2* transcription, we performed *ACTA2*–luciferase reporter gene assays in both MEFs and AoSMCs. As expected, the relative expression/stability of each *Purβ* construct in mammalian cells was similar to that seen in *E. coli*. Of the truncation proteins expressed, only the dimerization-competent *Purβ* I–II–III core construct and the *Purβ* I–II intramolecular subdomain were consistently found to repress both the complete and minimal *ACTA2* enhancer–promoter in both cell types (Figure 5 and Figure S8, Supporting Information). However, while *Purβ* I–II–III repressed the promoter to the same extent as the full-length protein, *Purβ* I–II exhibited ~50% less repressor activity. The intrinsically weaker activity of *Purβ* I–II was validated by titration experiments conducted over an extended range of expression vector concentrations pointing to the necessity of the PUR III repeat for full repressor function (Figure 6). Interestingly, forced expression of the *Purβ* III dimerization domain by itself did not affect the *ACTA2* enhancer–promoter owing, in part, to the apparent inability of this construct to enter the nucleus when separated from *Purβ* I–II intramolecular domain (Figure S11, Supporting Information). However, in the context of the full-length protein and the *Purβ* I–II–III core construct, we surmise that PUR repeat III likely promotes more efficient *ACTA2* repression by mediating the formation of a dimeric repressor capable of multisite ssDNA-binding within the confines of the nucleus.

Previous high-resolution structural analyses of the 5′-flanking region of *ACTA2* during myofibroblast differentiation revealed that an asymmetric Pur/Pyr tract spanning nucleotides –210 to –150 is hypersensitive to modification by chemical probes that preferentially react with unpaired nucleobases.<sup>58</sup> This region contains a consensus MCAT motif and a TGF- $\beta$ 1 response element that appear to function in conjunction with downstream CARG and GC boxes to mediate high-level *ACTA2* transcription in fibroblasts.<sup>16,17,20</sup> Consequently, we have chosen to focus our efforts on characterizing the interaction of *Purβ* with the MCAT region of the *ACTA2* enhancer–promoter due to its high Pur/Pyr asymmetry and apparent propensity to transiently adopt non-B-form structures *in vivo*.<sup>58</sup> In this regard, a prior study from our laboratory reported that *Purβ* interacts with the 32 nt purine-rich strand of the *ACTA2* MCAT element (dubbed PE32-F, –195 to –164) via a cooperative binding mechanism to generate a high-affinity 2:1 *Purβ*/ssDNA complex.<sup>37</sup>

To test the importance of protein dimerization in facilitating the interaction of *Purβ* with PE32-F, the relative ssDNA-binding affinity and specificity of full-length *Purβ* and the core

I–II–III protein were compared with the isolated intra- and intermolecular subdomains using both direct and competitive ssDNA-binding assays. Because these microplate-based colorimetric assays were performed under intrinsically nonequilibrium conditions, it was not possible to determine precise quantitative differences between Pur $\beta$  I–II–III and the full-length protein. Despite this technical limitation, the Pur $\beta$  I–II–III core construct did appear to bind PE32-F with comparable affinity and specificity to full-length Pur $\beta$  under the assay conditions employed (Figure 7). Moreover, the biochemical properties of Pur $\beta$  I–II–III (residues 41–303) defined in this study are analogous to those of a His tag-free core tryptic fragment of Pur $\beta$  (residues 29–305) described in an earlier report.<sup>40</sup> Interestingly, while the Pur $\beta$  I–II and Pur $\beta$  III subdomains each displayed a lower apparent affinity for PE32-F than Pur $\beta$  I–II–III, the intermolecular subdomain bound more tightly to ssDNA than the intramolecular subdomain. The functional nonidentity of the isolated Pur $\beta$  I–II and Pur $\beta$  III subdomains suggests that the native Pur $\beta$  homodimer contains three separate but unequal ssDNA-binding modules. This structural arrangement reinforces the concept that stable nucleoprotein complex assembly on the ACTA2 MCAT element likely involves the recognition of multiple binding sites by Pur $\beta$ .<sup>37</sup> In support of this assertion, mutation of all three PUR elements in PE32-F was necessary to completely eliminate ssDNA-binding by full-length Pur $\beta$ , the I–II–III core, and each subdomain (Figure 7D).

Another defining attribute of Pur $\beta$  structure and function uncovered in this report is that the individual subdomains of Pur $\beta$  differ in their capacity to interact with certain transcription factors relevant to ACTA2 regulation in fibroblasts. In particular, the Pur $\beta$  I–II intramolecular subdomain was a more avid binder of Sp3 than the Pur $\beta$  III intermolecular subdomain (Figure 8 and Figure S10, Supporting Information). Because Sp1 and Sp3 are known to interact with several sequence elements located within the composite MCAT/CAR/GC box enhancer,<sup>20</sup> it is quite possible that the relatively strong repressor activity of Pur $\beta$  I–II observed in transfected cells was due, in part, to its ability to bind and sequester Sp3 away from the enhancer. This would also explain why Pur $\beta$  I–II retained repressor activity in the face of its relatively weak ssDNA-binding affinity compared with Pur $\beta$  I–II–III. On the other hand, all three PUR repeats were required for efficient interaction of Pur $\beta$  with MSY1 (mouse YB-1), the co-repressor protein that interacts with the pyrimidine-rich antisense strand of the ACTA2 Pur/Pyr tract.<sup>17,22</sup> This feature may account for why Pur $\beta$  I–II–III was such an effective repressor when expressed in cells because direct physical interaction between Pur $\beta$  and MSY1 is probably essential for efficient assembly of these co-repressors on the Pur/Pyr element and ensuing disruption of the core MCAT motif.<sup>37</sup> Coordinated binding of MSY1 to the pyrimidine-rich strand may also serve to potentiate the intrinsic helix-destabilizing activity of Pur $\beta$ .<sup>28</sup> Unraveling the degree to which Pur $\beta$  can stably alter the secondary structure of specific *cis*-elements in ACTA2 will clearly require a more systematic evaluation of the helix-destabilizing properties of Pur $\beta$  and its isolated subdomains based on the biochemical criteria established for Pura-mediated melting of duplex DNA.<sup>27,28,69</sup>

In summary, our findings reveal that Pur $\beta$  is a potent inhibitor of myofibroblast differentiation by virtue of its ability to repress ACTA2 transcription via specific protein–ssDNA and protein–protein interactions. The functionally relevant

unit of Pur $\beta$  that mediates ACTA2 repression appears to be the homodimeric form of the protein. Subdomain-specific inter- and intramolecular interactions account for the formation of three separate ssDNA-binding modules within the Pur $\beta$  homodimer. The tripartite organization of the assembled homodimer readily explains the structural basis for the cooperative binding of Pur $\beta$  to multiple purine-rich sites within the MCAT region of the composite ACTA2 enhancer as well as the preferential association of Pur $\beta$  with its co-repressor partner MSY1/YB-1.

## ■ ASSOCIATED CONTENT

### ● Supporting Information

Table showing primer sets used in the amplification of cDNAs encoding mouse Pur $\beta$  truncation proteins, figures showing characterization of monoclonal antibodies recognizing Pura and Pur $\beta$ , growth of stably-transduced AKR-2B MEF cell lines, morphology of Pur $\beta$  knockdown MEFs at confluence, relative migration of Pur $\beta$  knockdown MEFs, hypothetical structure of PUR repeats I and II in Pura versus Pur $\beta$ , SDS-PAGE of purified Pur $\beta$  truncation proteins, analysis of Pur $\beta$  truncation proteins by CD spectroscopy, ACTA2 repressor activity of Pur $\beta$  truncation proteins expressed in C57BL/6 AoSMCs, binding of purified NHis-Pur $\beta$  proteins to PE32-bF, binding of AKR-2B MEF-derived transcription factors to purified NHis-Pur $\beta$  proteins, and subcellular distribution of Pur $\beta$  truncation proteins, and an expanded methods section. This material is available free of charge via the Internet at <http://pubs.acs.org>.

## ■ AUTHOR INFORMATION

### Corresponding Author

\*Mailing address: Department of Medicine, Cardiology/Vascular Biology Unit, University of Vermont College of Medicine, Colchester Research Facility, 208 South Park Drive, Colchester, VT 05446. Tel: (802) 656-0329. Fax: (802) 656-8969. E-mail: [robert.kelm@uvm.edu](mailto:robert.kelm@uvm.edu).

### Funding

This work was supported by NIH Grant R01 HL054281 and AHA Grant 09GRNT2170060 to R.J.K. A.E.R. and L.A.F. were supported by NIH Training Grant T32 HL007594 (Kenneth G. Mann, PI).

### Notes

The authors declare no competing financial interest.

## ■ ABBREVIATIONS

SMA $\alpha$ , smooth muscle  $\alpha$ -actin; ssDNA, single-stranded DNA; MEF, mouse embryo fibroblast; MCAT, muscle CAT motif; Pur/Pyr, polypurine/polypyrimidine; YB-1, Y-box binding protein 1; AoSMC, aortic outgrowth smooth muscle cell; TGF- $\beta$ 1, transforming growth factor  $\beta$ 1

## ■ REFERENCES

- (1) Walker, G. A., Guerrero, I. A., and Leinwand, L. A. (2001) Myofibroblasts: Molecular crossdressers. *Curr. Top. Dev. Biol.* 51, 91–107.
- (2) Tomasek, J. J., Gabbiani, G., Hinz, B., Chaponnier, C., and Brown, R. A. (2002) Myofibroblasts and mechano-regulation of connective tissue remodelling. *Nat. Rev. Mol. Cell Biol.* 3, 349–363.
- (3) Gabbiani, G., Ryan, G. B., and Majne, G. (1971) Presence of modified fibroblasts in granulation tissue and their possible role in wound contraction. *Experientia* 27, 549–550.

- (4) Gabbiani, G., Hirschel, B. J., Ryan, G. B., Statkov, P. R., and Majno, G. (1972) Granulation tissue as a contractile organ. A study of structure and function. *J. Exp. Med.* 135, 719–734.
- (5) Hinz, B. (2007) Formation and function of the myofibroblast during tissue repair. *J. Invest. Dermatol.* 127, 526–537.
- (6) Hinz, B., Phan, S. H., Thannickal, V. J., Galli, A., Bochaton-Piallat, M. L., and Gabbiani, G. (2007) The myofibroblast: One function, multiple origins. *Am. J. Pathol.* 170, 1807–1816.
- (7) De Wever, O., and Mareel, M. (2003) Role of tissue stroma in cancer cell invasion. *J. Pathol.* 200, 429–447.
- (8) Zaleski, A., Shi, Y., and Johnson, A. G. (2002) Diverse origin of intimal cells: smooth muscle cells, myofibroblasts, fibroblasts, and beyond? *Circ. Res.* 91, 652–655.
- (9) Hao, H., Gabbiani, G., Camenzind, E., Bacchetta, M., Virmani, R., and Bochaton-Piallat, M. L. (2006) Phenotypic modulation of intima and media smooth muscle cells in fatal cases of coronary artery lesion. *Arterioscler., Thromb., Vasc. Biol.* 26, 326–332.
- (10) Darby, I., Skalli, O., and Gabbiani, G. (1990) Alpha-smooth muscle actin is transiently expressed by myofibroblasts during experimental wound healing. *Lab. Invest.* 63, 21–29.
- (11) Wang, J., Zohar, R., and McCulloch, C. A. (2006) Multiple roles of alpha-smooth muscle actin in mechanotransduction. *Exp. Cell Res.* 312, 205–214.
- (12) Hinz, B., Celetta, G., Tomasek, J. J., Gabbiani, G., and Chaponnier, C. (2001) Alpha-smooth muscle actin expression upregulates fibroblast contractile activity. *Mol. Biol. Cell* 12, 2730–2741.
- (13) Stoflet, E. S., Schmidt, L. J., Elder, P. K., Korf, G. M., Foster, D. N., Strauch, A. R., and Getz, M. J. (1992) Activation of a muscle-specific actin gene promoter in serum-stimulated fibroblasts. *Mol. Biol. Cell* 3, 1073–1083.
- (14) Foster, D. N., Min, B., Foster, L. K., Stoflet, E. S., Sun, S., Getz, M. J., and Strauch, A. R. (1992) Positive and negative cis-acting regulatory elements mediate expression of the mouse vascular smooth muscle alpha-actin gene. *J. Biol. Chem.* 267, 11995–12003.
- (15) Sun, S., Stoflet, E. S., Cogan, J. G., Strauch, A. R., and Getz, M. J. (1995) Negative regulation of the vascular smooth muscle alpha-actin gene in fibroblasts and myoblasts: disruption of enhancer function by sequence-specific single-stranded-DNA-binding proteins. *Mol. Cell. Biol.* 15, 2429–2436.
- (16) Subramanian, S. V., Polikandriotis, J. A., Kelm, R. J., Jr., David, J. J., Orosz, C. G., and Strauch, A. R. (2004) Induction of vascular smooth muscle alpha-actin gene transcription in transforming growth factor beta1-activated myofibroblasts mediated by dynamic interplay between the Pur repressor proteins and Sp1/Smad coactivators. *Mol. Biol. Cell* 15, 4532–4543.
- (17) Carlini, L. E., Getz, M. J., Strauch, A. R., and Kelm, R. J., Jr. (2002) Cryptic MCAT enhancer regulation in fibroblasts and smooth muscle cells. Suppression of TEF-1 mediated activation by the single-stranded DNA-binding proteins, Pur alpha, Pur beta, and MSY1. *J. Biol. Chem.* 277, 8682–8692.
- (18) Gan, Q., Yoshida, T., Li, J., and Owens, G. K. (2007) Smooth muscle cells and myofibroblasts use distinct transcriptional mechanisms for smooth muscle alpha-actin expression. *Circ. Res.* 101, 883–892.
- (19) Sandbo, N., Kregel, S., Taurin, S., Bhorade, S., and Dulin, N. O. (2009) Critical role of serum response factor in pulmonary myofibroblast differentiation induced by TGF-beta. *Am. J. Respir. Cell Mol. Biol.* 41, 332–338.
- (20) Cogan, J. G., Subramanian, S. V., Polikandriotis, J. A., Kelm, R. J., Jr., and Strauch, A. R. (2002) Vascular smooth muscle alpha-actin gene transcription during myofibroblast differentiation requires Sp1/3 protein binding proximal to the MCAT enhancer. *J. Biol. Chem.* 277, 36433–36442.
- (21) Cogan, J. G., Sun, S., Stoflet, E. S., Schmidt, L. J., Getz, M. J., and Strauch, A. R. (1995) Plasticity of vascular smooth muscle alpha-actin gene transcription. Characterization of multiple, single-, and double-strand specific DNA-binding proteins in myoblasts and fibroblasts. *J. Biol. Chem.* 270, 11310–11321.
- (22) Kelm, R. J., Jr., Cogan, J. G., Elder, P. K., Strauch, A. R., and Getz, M. J. (1999) Molecular interactions between single-stranded DNA-binding proteins associated with an essential MCAT element in the mouse smooth muscle alpha-actin promoter. *J. Biol. Chem.* 274, 14238–14245.
- (23) Bergemann, A. D., and Johnson, E. M. (1992) The HeLa Pur factor binds single-stranded DNA at a specific element conserved in gene flanking regions and origins of DNA replication. *Mol. Cell. Biol.* 12, 1257–1265.
- (24) Bergemann, A. D., Ma, Z. W., and Johnson, E. M. (1992) Sequence of cDNA comprising the human pur gene and sequence-specific single-stranded-DNA-binding properties of the encoded protein. *Mol. Cell. Biol.* 12, 5673–5682.
- (25) Johnson, E. M., Daniel, D. C., and Gordon, J. (2013) The pur protein family: Genetic and structural features in development and disease. *J. Cell. Physiol.* 228, 930–937.
- (26) Kelm, R. J., Jr., Elder, P. K., Strauch, A. R., and Getz, M. J. (1997) Sequence of cDNAs encoding components of vascular actin single-stranded DNA-binding factor 2 establish identity to Puralpha and Purbeta. *J. Biol. Chem.* 272, 26727–26733.
- (27) Darbinian, N., Gallia, G. L., and Khalili, K. (2001) Helix-destabilizing properties of the human single-stranded DNA- and RNA-binding protein Puralpha. *J. Cell. Biochem.* 80, 589–595.
- (28) Wortman, M. J., Johnson, E. M., and Bergemann, A. D. (2005) Mechanism of DNA binding and localized strand separation by Pur alpha and comparison with Pur family member, Pur beta. *Biochim. Biophys. Acta* 1743, 64–78.
- (29) Kelm, R. J., Jr., Wang, S. X., Polikandriotis, J. A., and Strauch, A. R. (2003) Structure/function analysis of mouse Purbeta, a single-stranded DNA-binding repressor of vascular smooth muscle alpha-actin gene transcription. *J. Biol. Chem.* 278, 38749–38757.
- (30) Knapp, A. M., Ramsey, J. E., Wang, S. X., Godburn, K. E., Strauch, A. R., and Kelm, R. J., Jr. (2006) Nucleoprotein interactions governing cell type-dependent repression of the mouse smooth muscle alpha-actin promoter by single-stranded DNA-binding proteins Pur alpha and Pur beta. *J. Biol. Chem.* 281, 7907–7918.
- (31) Gupta, M., Sueblinvong, V., Raman, J., Jeevanandam, V., and Gupta, M. P. (2003) Single-stranded DNA-binding proteins PURalpha and PURbeta bind to a purine-rich negative regulatory element of the alpha-myosin heavy chain gene and control transcriptional and translational regulation of the gene expression. Implications in the repression of alpha-myosin heavy chain during heart failure. *J. Biol. Chem.* 278, 44935–44948.
- (32) Ji, J., Tsika, G. L., Rindt, H., Schreiber, K. L., McCarthy, J. J., Kelm, R. J., Jr., and Tsika, R. (2007) Puralpha and Purbeta collaborate with Sp3 to negatively regulate beta-myosin heavy chain gene expression during skeletal muscle inactivity. *Mol. Cell. Biol.* 27, 1531–1543.
- (33) Gupta, M., Sueblinvong, V., and Gupta, M. P. (2007) The single-strand DNA/RNA-binding protein, Purbeta, regulates serum response factor (SRF)-mediated cardiac muscle gene expression. *Can. J. Physiol. Pharmacol.* 85, 349–359.
- (34) McCarthy, J. J., Esser, K. A., Peterson, C. A., and Dupont-Versteegden, E. E. (2009) Evidence of MyomiR network regulation of beta-myosin heavy chain gene expression during skeletal muscle atrophy. *Physiol. Genomics* 39, 219–226.
- (35) van Rooij, E., Quiat, D., Johnson, B. A., Sutherland, L. B., Qi, X., Richardson, J. A., Kelm, R. J., Jr., and Olson, E. N. (2009) A family of microRNAs encoded by myosin genes governs myosin expression and muscle performance. *Dev. Cell* 17, 662–673.
- (36) Ramsey, J. E., Daugherty, M. A., and Kelm, R. J., Jr. (2007) Hydrodynamic studies on the quaternary structure of recombinant mouse Purbeta. *J. Biol. Chem.* 282, 1552–1560.
- (37) Ramsey, J. E., and Kelm, R. J., Jr. (2009) Mechanism of strand-specific smooth muscle alpha-actin enhancer interaction by purine-rich element binding protein B (Purbeta). *Biochemistry* 48, 6348–6360.
- (38) Graebisch, A., Roche, S., Kostrewa, D., Soding, J., and Niessing, D. (2010) Of bits and bugs—on the use of bioinformatics and a



bacterial crystal structure to solve a eukaryotic repeat-protein structure. *PLoS One* 5, No. e13402.

(39) Graebisch, A., Roche, S., and Niessing, D. (2009) X-ray structure of Pur-alpha reveals a Whirly-like fold and an unusual nucleic-acid binding surface. *Proc. Natl. Acad. Sci. U. S. A.* 106, 18521–18526.

(40) Rumora, A. E., Steere, A. N., Ramsey, J. E., Knapp, A. M., Ballif, B. A., and Kelm, R. J., Jr. (2010) Isolation and characterization of the core single-stranded DNA-binding domain of purine-rich element binding protein B (Purbeta). *Biochem. Biophys. Res. Commun.* 400, 340–345.

(41) Wang, J., Niu, W., Nikiforov, Y., Naito, S., Chernauek, S., Witte, D., LeRoith, D., Strauch, A., and Fagin, J. A. (1997) Targeted overexpression of IGF-I evokes distinct patterns of organ remodeling in smooth muscle cell tissue beds of transgenic mice. *J. Clin. Invest.* 100, 1425–1439.

(42) Larkin, M. A., Blackshields, G., Brown, N. P., Chenna, R., McGettigan, P. A., McWilliam, H., Valentin, F., Wallace, I. M., Wilm, A., Lopez, R., Thompson, J. D., Gibson, T. J., and Higgins, D. G. (2007) Clustal W and Clustal X version 2.0. *Bioinformatics* 23, 2947–2948.

(43) Goujon, M., McWilliam, H., Li, W., Valentin, F., Squizzato, S., Paern, J., and Lopez, R. (2010) A new bioinformatics analysis tools framework at EMBL-EBI. *Nucleic Acids Res.* 38, W695–699.

(44) Biegert, A., and Soding, J. (2008) De novo identification of highly diverged protein repeats by probabilistic consistency. *Bioinformatics* 24, 807–814.

(45) Buchan, D. W., Ward, S. M., Loble, A. E., Nugent, T. C., Bryson, K., and Jones, D. T. (2010) Protein annotation and modelling servers at University College London. *Nucleic Acids Res.* 38, W563–568.

(46) Zhang, Y. (2008) I-TASSER server for protein 3D structure prediction. *BMC Bioinf.* 9, No. 40.

(47) Roy, A., Kucukural, A., and Zhang, Y. (2010) I-TASSER: A unified platform for automated protein structure and function prediction. *Nat. Protoc.* 5, 725–738.

(48) Arnold, K., Bordoli, L., Kopp, J., and Schwede, T. (2006) The SWISS-MODEL workspace: A web-based environment for protein structure homology modelling. *Bioinformatics* 22, 195–201.

(49) Kiefer, F., Arnold, K., Kunzli, M., Bordoli, L., and Schwede, T. (2009) The SWISS-MODEL Repository and associated resources. *Nucleic Acids Res.* 37, D387–392.

(50) Bordoli, L., Kiefer, F., Arnold, K., Benkert, P., Battey, J., and Schwede, T. (2009) Protein structure homology modeling using SWISS-MODEL workspace. *Nat. Protoc.* 4, 1–13.

(51) Emsley, P., Lohkamp, B., Scott, W. G., and Cowtan, K. (2010) Features and development of Coot. *Acta Crystallogr., Sect. D: Biol. Crystallogr.* 66, 486–501.

(52) Brunger, A. T., Adams, P. D., Clore, G. M., DeLano, W. L., Gros, P., Grosse-Kunstleve, R. W., Jiang, J. S., Kuszewski, J., Nilges, M., Pannu, N. S., Read, R. J., Rice, L. M., Simonson, T., and Warren, G. L. (1998) Crystallography & NMR system: A new software suite for macromolecular structure determination. *Acta Crystallogr., Sect. D: Biol. Crystallogr.* 54, 905–921.

(53) Brunger, A. T. (2007) Version 1.2 of the Crystallography and NMR system. *Nat. Protoc.* 2, 2728–2733.

(54) Schrödinger, LLC. (2010) The PyMOL Molecular Graphics System, Version 1.3r1.

(55) Gasteiger, E., Gattiker, A., Hoogland, C., Ivanyi, I., Appel, R. D., and Bairoch, A. (2003) ExPASy: The proteomics server for in-depth protein knowledge and analysis. *Nucleic Acids Res.* 31, 3784–3788.

(56) Knapp, A. M., Ramsey, J. E., Wang, S. X., Strauch, A. R., and Kelm, R. J., Jr. (2007) Structure-function analysis of mouse Pur beta II. Conformation altering mutations disrupt single-stranded DNA and protein interactions crucial to smooth muscle alpha-actin gene repression. *J. Biol. Chem.* 282, 35899–35909.

(57) Wang, S. X., Elder, P. K., Zheng, Y., Strauch, A. R., and Kelm, R. J., Jr. (2005) Cell cycle-mediated regulation of smooth muscle alpha-actin gene transcription in fibroblasts and vascular smooth muscle cells

involves multiple adenovirus E1A-interacting cofactors. *J. Biol. Chem.* 280, 6204–6214.

(58) Becker, N. A., Kelm, R. J., Jr., Vrana, J. A., Getz, M. J., and Maher, L. J., 3rd (2000) Altered sensitivity to single-strand-specific reagents associated with the genomic vascular smooth muscle alpha-actin promoter during myofibroblast differentiation. *J. Biol. Chem.* 275, 15384–15391.

(59) White, M. K., Johnson, E. M., and Khalili, K. (2009) Multiple roles for Puralpha in cellular and viral regulation. *Cell Cycle* 8, 1–7.

(60) Ronnov-Jessen, L., and Petersen, O. W. (1996) A function for filamentous alpha-smooth muscle actin: retardation of motility in fibroblasts. *J. Cell Biol.* 134, 67–80.

(61) Hinz, B., Phan, S. H., Thannickal, V. J., Prunotto, M., Desmouliere, A., Varga, J., De Wever, O., Mareel, M., and Gabbiani, G. (2012) Recent developments in myofibroblast biology: paradigms for connective tissue remodeling. *Am. J. Pathol.* 180, 1340–1355.

(62) Zhang, A., David, J. J., Subramanian, S. V., Liu, X., Fuerst, M. D., Zhao, X., Leier, C. V., Orosz, C. G., Kelm, R. J., Jr., and Strauch, A. R. (2008) Serum response factor neutralizes Pur alpha- and Pur beta-mediated repression of the fetal vascular smooth muscle alpha-actin gene in stressed adult cardiomyocytes. *Am. J. Physiol.: Cell Physiol.* 294, C702–714.

(63) Johnson, E. M., Chen, P. L., Krachmarov, C. P., Barr, S. M., Kanovsky, M., Ma, Z. W., and Lee, W. H. (1995) Association of human Pur alpha with the retinoblastoma protein, Rb, regulates binding to the single-stranded DNA Pur alpha recognition element. *J. Biol. Chem.* 270, 24352–24360.

(64) Barr, S. M., and Johnson, E. M. (2001) Ras-induced colony formation and anchorage-independent growth inhibited by elevated expression of Puralpha in NIH3T3 cells. *J. Cell. Biochem.* 81, 621–638.

(65) Khalili, K., Del Valle, L., Muralidharan, V., Gault, W. J., Darbinian, N., Otte, J., Meier, E., Johnson, E. M., Daniel, D. C., Kinoshita, Y., Amini, S., and Gordon, J. (2003) Puralpha is essential for postnatal brain development and developmentally coupled cellular proliferation as revealed by genetic inactivation in the mouse. *Mol. Cell. Biol.* 23, 6857–6875.

(66) Liu, H., Barr, S. M., Chu, C., Kohtz, D. S., Kinoshita, Y., and Johnson, E. M. (2005) Functional interaction of Puralpha with the Cdk2 moiety of cyclin A/Cdk2. *Biochem. Biophys. Res. Commun.* 328, 851–857.

(67) Darbinian, N., Gallia, G. L., Kundu, M., Shcherbik, N., Tretiakova, A., Giordano, A., and Khalili, K. (1999) Association of Pur alpha and E2F-1 suppresses transcriptional activity of E2F-1. *Oncogene* 18, 6398–6402.

(68) Darbinian, N., White, M. K., Gallia, G. L., Amini, S., Rappaport, J., and Khalili, K. (2004) Interaction between the pura and E2F-1 transcription factors. *Anticancer Res.* 24, 2585–2594.

(69) Zhang, Q., Pedigo, N., Shenoy, S., Khalili, K., and Kaetzel, D. M. (2005) Puralpha activates PDGF-A gene transcription via interactions with a G-rich, single-stranded region of the promoter. *Gene* 348, 25–32.